

Hierarchical macroporous–mesoporous SBA-15 sulfonic acid catalysts for biodiesel synthesis†

Jérémy Dhainaut, Jean-Philippe Dacquin, Adam F. Lee* and Karen Wilson*

Received 17th September 2009, Accepted 10th November 2009

First published as an Advance Article on the web 16th December 2009

DOI: 10.1039/b919341c

Hierarchical macroporous–mesoporous SBA-15 silicas have been synthesised *via* dual-templating routes employing liquid crystalline surfactants and polystyrene beads. These offer high surface areas and well-defined, interconnecting macro- and mesopore networks with respective narrow size distributions around 300 nm and 3–5 nm for polystyrene:tetraethoxysilane ratios $\geq 2:1$. Subsequent functionalisation with propylsulfonic acid yields the first organized, macro-mesoporous solid acid catalyst. The enhanced mass transport properties of these new bi-modal solid acid architectures confer significant rate enhancements in the transesterification of bulky glyceryl trioctanoate, and esterification of long chain palmitic acid, over pure mesoporous analogues. This paves the way to the wider application of hierarchical catalysts in biofuel synthesis and biomass conversion.

Introduction

The International Energy Agency predicts a 55% increase in global fuel consumption by the year 2030,¹ principally the result of the growing needs of emerging nations. The combination of dwindling oil reserves and growing concerns over carbon dioxide emissions and associated climate change is driving the urgent development of clean, sustainable energy supplies. Biomass offers a partial solution to the replacement of fossil fuels for the production of key chemical feedstocks and transportation fuels such as ethanol and biodiesel. First generation alternative biofuels have proven controversial due to their synthesis from important food crops including corn, sugarcane and palm or rapeseed oils, and consequent impact on global food prices. Recent focus has therefore shifted towards so-called second generation non-food biomass sources like cellulose, algae or non-edible plant oils from the Euphorbiaceae family² (notably *Jatropha* or *Castor* oil), which do not compete with traditional agronomies.

Biodiesel sourced from renewable second generation crops is non-toxic and biodegradable, with the potential for closed CO₂ cycles³ and thus vastly reduced carbon footprints compared with petroleum fuels.^{3,4} It comprises long chain fatty acid methyl esters (FAMES), typically derived from vegetable oils or animal fats rich in triacyl glycerides (TAGs) and free fatty acids (FFAs).⁵ The transesterification of oil seed TAGs to methyl (or ethyl) esters can be catalyzed by acids or bases, and the vast majority of biodiesel is currently produced *via* homogeneous catalysis, using soluble bases such as NaOH/NaOMe or KOH.^{6,7} Although liquid base catalysts offer high transesterification rates, they

are sensitive to water and FFA impurities which are always present in trace amounts even in refined plant oils. FFA removal from biodiesel is essential in order to prevent corrosion of vehicle fuel tanks and engine blocks, and is currently achieved through an acid catalyzed esterification pretreatment step prior to transesterification. Simultaneous FFA esterification and TAG transesterification using acid catalysts provides an alternative single step (albeit high temperature) process for poor quality oils containing high FFA levels.^{5,6,8–10} However, in both scenarios reactor corrosion and removal of soluble catalyst species from the resulting biofuel mixture is particularly problematic, requiring aqueous quench and neutralisation steps which themselves generate undesired emulsions and soap formation.^{6,11} The resultant *E*-factor (defined as the [total waste]/[product] ratio) is concomitantly poor due to catalyst losses after each reaction and the production of copious contaminated water. Furthermore, the major by-product of biodiesel synthesis, glycerol, is heavily contaminated by homogeneous catalyst residues and/or water and therefore of little re-sale value to potential consumers in the cosmetic, food and pharmaceutical industries.

Non-corrosive heterogeneous catalysts that are easily recovered and recyclable could greatly improve the environmental impact of commercial biodiesel processing, eliminating the need for aqueous quench cycles while offering the opportunity for continuous operation in flow reactors.^{5,6,11,12} Diverse solid acids and bases including zeolites,¹³ resins,¹⁴ alkali earth oxides,^{15–17} hydrotalcites¹⁸ and calcined dolomitic rock¹⁹ have been investigated for TAG transesterification and their application recently reviewed.^{4,5,6,12} Unfortunately, the micro and mesoporous catalyst systems investigated to date are not optimal for the bulky and viscous C₁₆–C₁₈ TAGs typical of plant oils.²⁰ Even tailored, large pore (>4–15 nm) mesoporous catalysts based upon SBA-15²¹ that are active for esterification and transesterification,^{9,22–25} often possess long, isolated parallel channels resulting in slow in-pore diffusion and correspondingly slow turnover. Current material syntheses have focused solely on generating and tuning mesoporosity, largely

School of Chemistry, Cardiff University, Cardiff, UK CF10 3AT.
E-mail: leeaf@cardiff.ac.uk, wilsonk5@cardiff.ac.uk; Fax: 44 2920 870827; Tel: 44 2920 874030

† Electronic supplementary information (ESI) available: PS bead characterization and comparative textural properties of pre- and post-functionalized silicas. See DOI: 10.1039/b919341c

ignoring the benefits of hierarchical porous networks containing macropores to act as rapid transport conduits to the active sites. Simulations show that in the Knudsen diffusion regime,²⁶ where reactants/products are able to enter/exit mesopores but experience attendant diffusion limitations, such bi-modal pore structures could significantly improve catalyst activity. Catalytically active materials possessing such interconnecting macropore–mesopore networks²⁷ with well-defined dimensions would be particularly suited to boosting mass-transport in viscous liquid phase reactions such as biodiesel synthesis. They can be prepared using microemulsion,²⁸ colloidal polystyrene microspheres²⁹ or co-surfactants³⁰ routes in conjunction with mesoporous templates, and are particularly attractive for application in liquid continuous flow reactors wherein rapid pore diffusion is required. Polystyrene microspheres allow great control over the final macropore properties. SBA-15 silicas have been recently synthesised incorporating macropores of a few hundred nanometres by the use of these templating polymers,^{31–33} offering high specific surface areas and improved diffusion characteristics, but to our knowledge have yet to be applied in heterogeneous catalysis.

Surface grafting of alkoxy silanes offers a convenient method to covalently attach organic functional groups to porous silica frameworks without the risk of pore blockage or leaching of the grafted component.³⁴ Sulfonic acid silicas are a class of solid Brønsted acid catalyst comprising tethered organo-sulfonic acid groups^{35–37} that provide alternatives to commercially available sulfonated polymer resins, such as Amberlyst-15 and Nafion-H. In this paper we explore the use of grafting to attach pure Brønsted acid sites to macroporous–mesoporous SBA-15 supports and thereby generate a new class of ordered, hierarchical sulfonic acid functionalised silicas, designed specifically for bulky plant oils. Macropore inclusion significantly enhances the rate of both C₈ TAG transesterification to FAME and C₁₆ FFA esterification with methanol.

Experimental

Polystyrene bead synthesis

The emulsion polymerisation approach of Vaudreuil and co-workers was adopted to generate monodisperse polystyrene (PS) beads.³⁸ 0.083 g of potassium persulfate (99%, Sigma-Aldrich) was dissolved in 6 ml of deionized water and dried at 70 °C. Separately, 239.5 ml of deionized water was added to a 500 ml three-neck round-bottom flask and heated to 70 °C under N₂. 25 ml of styrene (99%, Sigma-Aldrich) and 4.75 ml of divinylbenzene (80%, Sigma-Aldrich) was washed three times in a separating funnel with a 0.1 M NaOH solution (pellets, Sigma-Aldrich) and deionized water to remove polymerization inhibitors. The styrene and divinylbenzene were transferred to the 500 ml temperature stabilized flask, along with 26 ml of deionized water used to wash out the funnel. The potassium persulfate was then added to initiate styrene polymerization, and 15 h later the resultant white solution was filtered, then washed three times with deionized water and three times with ethanol. The final beads possessed a narrow size distribution of ~320 nm diameter (Figures S1 and 2†), while thermo-gravimetric analysis

(TGA) revealed their complete decomposition in air at 550 °C (Figure S3†).

SBA-15 synthesis

Macroporous–mesoporous SBA-15 silicas were synthesized following the approach of Zhao *et al.*,³⁹ with the addition of polystyrene beads during the synthesis to create macropores.^{31,32,33} Typically, 1.0 g of Pluronic P123 triblock copolymer was dissolved in 7.5 ml of water and 25 ml of 2 M HCl solution (Fisher) while stirring at 35 °C. The required amount of polystyrene beads for the appropriate PS:tetraethoxysilane (TEOS 98%, Sigma-Aldrich) mass ratio were then added to the solution and stirred for an hour. Once a good dispersion of PS beads was achieved, 2.3 ml of TEOS were added to the solution, which was maintained at 35 °C for 24 h while stirring. The mixture was then aged at 80 °C for 24 h and the solid product filtered, washed 3 times with deionised water, and calcined statically in air at 550 °C (ramp rate of 0.5 °C min⁻¹) for 6 h. The final solids are termed MM-SBA15-X, where X = PS:TEOS weight ratio.

Sulfonic acid functionalization

Sulfonic acid functionalization was performed by post-synthesis grafting as described previously.^{9,40,41} A mixture of 0.5 g of MM-SBA15-X and 0.50 ml of 3-mercaptopropyl trimethoxysilane (MPTMS 95%, Alfa Aesar) in 15 ml of toluene (Fisher) was refluxed at 130 °C for 24 h, and the resulting thiol-functionalized solid filtered, washed 3 times with methanol (Fisher) and dried at 80 °C overnight. Thiol groups were converted to –SO₃H by mild oxidation with 10 ml of 30% hydrogen peroxide (Sigma-Aldrich) by continuous stirring at room temperature for 24 h. Sulfonated MM-SBA15-X solid was subsequently filtered, washed 3 times with methanol, and dried at 80 °C overnight.

Glyceryl trioctanoate transesterification

Transesterification was performed at 60 °C under stirring using 0.05 g of catalyst, 4.92 ml of glyceryl trioctanoate (commercial name tricaprylin 99%, Sigma-Aldrich), 0.59 ml of dihexylether (Fisher) as an internal standard, and 12.50 ml of methanol, giving a MeOH:TAG ratio of 30:1. Aliquots of 0.1 ml were regularly sampled and analyzed by gas chromatography using a Varian 450-GC equipped with a VF-1ms 25 m × 0.25 mm capillary column. Product yields were calculated using response factors derived for methyl octanoate (99%, Fluka).

Palmitic acid esterification

Esterification was performed at 60 °C under stirring using 0.05 g of catalyst, 2.564 g (10 mmol) of palmitic acid (Sigma-Aldrich), 0.59 ml (2.5 mmol) of dihexylether and 12.50 ml (300 mmol) of methanol. Aliquots of 0.1 ml were regularly sampled and analyzed using a Varian 3900 GC equipped with a CP-Sil 5CB, 15 m × 0.25 mm capillary column. Product yields were calculated using response factors derived for methyl palmitate (99%, Sigma-Aldrich).

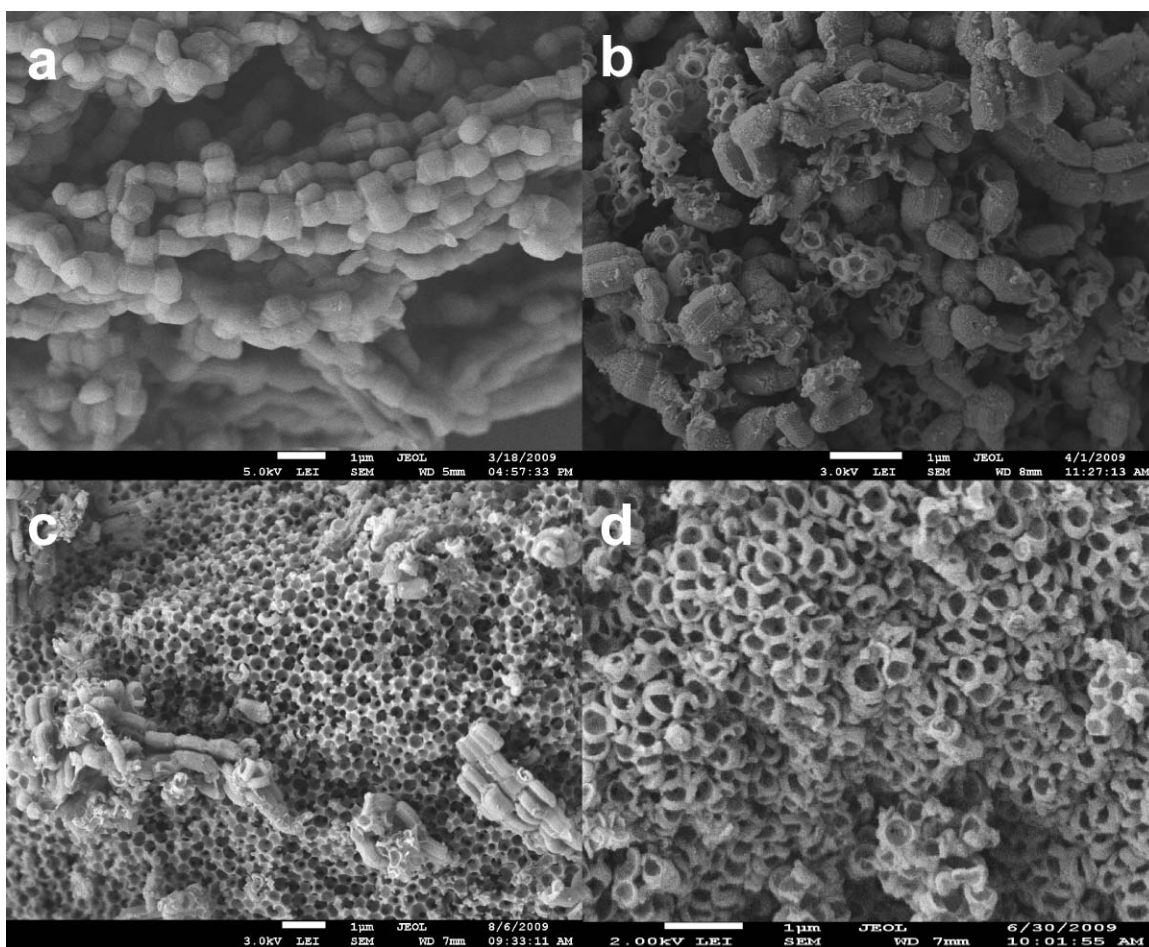


Fig. 1 SEM images of: a) SBA-15; b) MM-SBA15-1; c) MM-SBA15-2 and d) MM-SBA15-4 hierarchical macroporous-mesoporous silicas.

Material characterization

Powder X-ray diffraction patterns were collected on a Bruker D8 Advance diffractometer fitted with a Lynx eye high-speed strip detector and Cu-K α radiation source. Small-angle patterns were recorded from 0.65° to 3° with 0.02° steps at 10 s per point. Sulfur content was determined using an Horiba XGT-7000 X-Ray Fluorescence spectrometer. Nitrogen porosimetry was performed on a Quantasorb Nova 1200 instrument, after sample evacuation at 200 °C for 4 h. Surface areas were calculated using the Brunauer-Emmet-Teller (BET) method over the range $P/P_0 = 0.075-0.35$, where a linear relationship is maintained. Pore size distributions were calculated using the Barrett-Joyner-Halenda (BJH) model applied to the desorption isotherm branch. Mesopore volumes were evaluated at $P/P_0 = 0.98$. SEM was conducted on a JEOL JSM 7500F system; samples were gold coated prior to analysis. High-resolution TEM was carried out on a JEOL 2011 operating at 200 kV; samples were deposited from ethanolic solution onto holey-carbon copper grids. XPS measurements were performed using a Kratos AXIS HSi instrument equipped with a charge neutraliser and Mg-K α X-ray source. TGA was performed using a Stanton Redcroft STA 780 thermal analyser at 10 °C min⁻¹ under flowing He/O₂ (80:20 v/v) or He (20 ml min⁻¹ total) for template removal and sulfonic acid decomposition studies respectively.

Results and discussion

Materials characterization

A series of macro-mesostructured derived silicas were first prepared using different PS:TEOS ratios to incorporate macropores within the conventional SBA-15 mesopore framework. These are denoted MM-SBA15-1, MM-SBA15-2 and MM-SBA15-4 corresponding to 1:1, 2:1 and 4:1 weight ratios of PS beads to TEOS. A pure mesoporous SBA-15 silica was also synthesised for comparison. The morphology and porosity of these materials were explored *via* electron microscopy to confirm successful macropore incorporation. SEM of the undoped SBA-15 reveals a bead-like morphology characteristic of this class of material (Fig. 1).⁴² The addition of PS beads progressively modifies the SBA-15-like organization, creating a new morphology comprising two distinct structures for the intermediate MM-SBA15-1 and MM-SBA15-2 samples, which evolve into a more uniform macroporous network for MM-SBA15-4. The macropores in MM-SBA15-2 and MM-SBA15-4 are very regular, with average diameters around 300 nm, close to the parent PS bead dimensions. This contrasts with previous reports³³ wherein notable macropore shrinkage was observed after calcination, and likely reflects the slower heating rate used in the present study. It is also interesting to note that the

macropores are open and interconnected and thus well-suited to promote rapid through particle diffusion.

Mesopore character was evaluated by TEM which shows that the typical 2D periodic hexagonal structure of SBA-15 was retained in all cases, while the introduction of macropores, as anticipated (and desired) breaks up extended mesoporous channels. Fig. 2a demonstrates how the macropore framework silica is composed of highly-organized concentric mesoporous channels, resulting from self-assembly of the block copolymer solution around polystyrene beads. Hexagonal ordering of the mesopore channels is also clearly visible at higher magnification (Fig. 2b and 2c), with a mean lattice parameter (a_0) of 11.2 nm measured for the purely mesoporous SBA-15, and a slight decrease to 10.0 nm observed as the degree of macroporosity increases.† The high curvature of mesoporous channels in MM-SBA-4 suggests that strong electrostatic and hydrogen-bonding interactions³¹ between polystyrene beads, the block co-polymer and silica precursor promote self assembly of templated, mesostructured channels around the physical PS bead template. This curvature, presumably arising from strain on the block co-polymer layers of the liquid crystal template phase in conforming to the PS bead morphology, may account

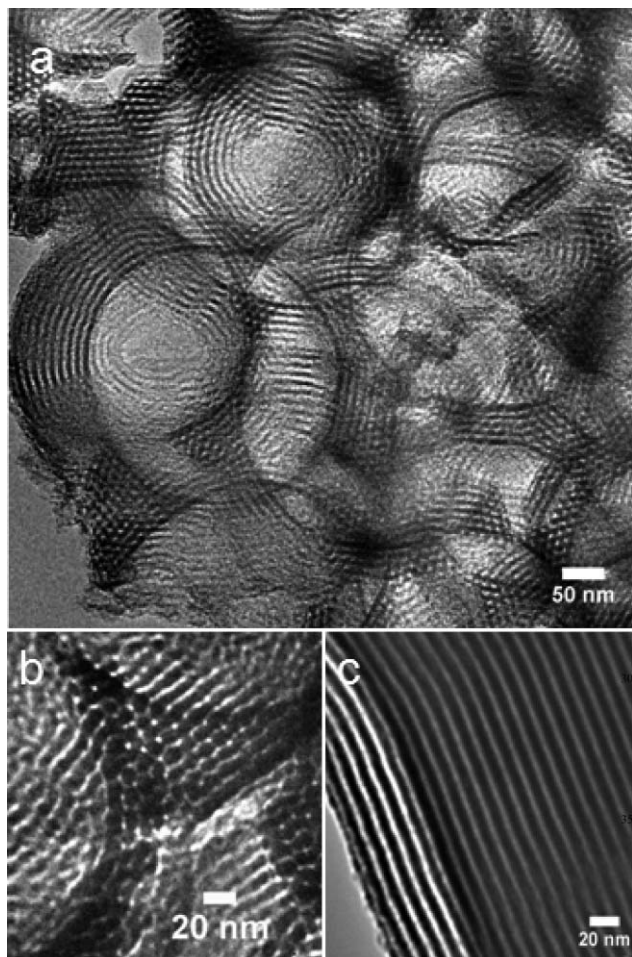


Fig. 2 HRTEM of: a) hierarchical macro and mesopore structures in MM-SBA15-4; b) high resolution image of hexagonal mesoporous arrays in MM-SBA15-4 and c) mesoporous channels in MM-SBA15-2.

for the slightly contracted mesoporous channels observed in the hierarchical materials (Figure S4†).

Long range ordering and porosity were subsequently investigated by XRD and N_2 porosimetry. Fig. 3 presents low angle diffraction patterns which evidence a major reflection at $2\theta \sim 0.9^\circ$ for all samples, characteristic of a periodic mesopore framework. Calcined SBA-15 material exhibits well defined peaks at 0.98 , 1.57 and 1.81° , associated with the (100), (110) and (200) planes of the P6mm space group for the hexagonal arrangement of mesoporous channels.^{39,43,44} Macropore incorporation slightly shifts diffraction peaks to higher angles, corresponding to a contraction in the mesopore lattice parameter from 11.2 to 10 nm. Increasing PS loading is also accompanied by attenuation and broadening of the d_{100} peak; line broadening analysis (Table 1) indicates a progressive decrease in the average mesopore domain size from 98 to 35 nm upon macropore inclusion, consistent with localisation of mesopore domains solely in the walls of the macropore framework as observed by HRTEM (Fig. 2a). Porosimetry shows all materials exhibit Type IV adsorption isotherms with type-H1 hysteresis loops characteristic of bottlenecked pore openings evident in Fig. 4. The loop size decreases with increasing macropore character, which may be accounted for by disruption of extended mesopore networks⁴⁵ that typically limit diffusion and impart hysteresis in the desorption isotherm branch. Additional prominent hysteresis observed above $P/P_0 = 0.9$ for MM-SBA15-4 is attributed to the high concentration of

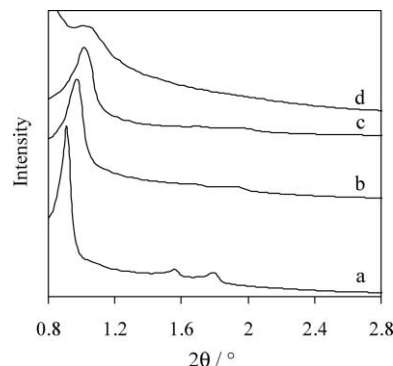


Fig. 3 Low angle powder XRD patterns of: a) SBA-15; b) MM-SBA15-1; c) MM-SBA15-2 and d) MM-SBA15-4 hierarchical macroporous-mesoporous silicas.

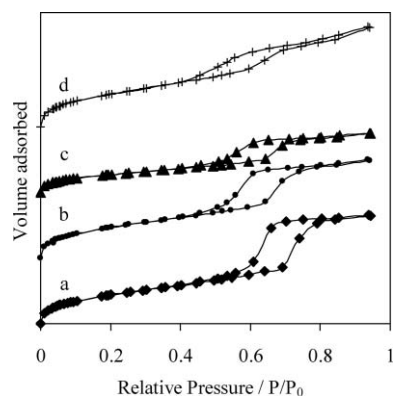


Fig. 4 Nitrogen adsorption-desorption isotherms of a) SBA-15; b) MM-SBA15-1; c) MM-SBA15-2 and d) MM-SBA15-4 hierarchical macroporous-mesoporous silicas.

Table 1 Physical and structural properties of selected *meso* and macro-mesoporous silica

Sample	Surface area ^a /m ² g ⁻¹	Mesopore volume ^b /cm ³ g ⁻¹	BJH pore diameter ^c /nm	d ₁₀₀ ^d /nm	Wall thickness ^e /nm	Mesopore domain size ^f /nm
SBA-15	974	1.08 (1.18)	5.8	9.73	5.4	98.2
MM-SBA15-1	976	0.82 (1.07)	5.0	9.17	5.6	74.3
MM-SBA15-2	971	0.87 (0.99)	4.5	8.68	5.0	55.2
MM-SBA15-4	938	0.84 (1.15)	3.9	8.68	6.1	34.6

^a Evaluated by multi-point BET method. ^b BJH mesopore volumes from the desorption isotherm, and total pore volume shown in brackets. ^c BJH average pore diameters from desorption isotherm. ^d Interlayer spacing derived from Bragg's Law. ^e Wall thickness = (2d₁₀₀/√3) – pore diameter. ^f Calculated from Scherrer equation.

macropores interconnected *via* bottlenecks.⁴⁵ Porosimetry also confirms shrinkage of the mesopore diameter with increased macropore character, shown in Fig. 5.

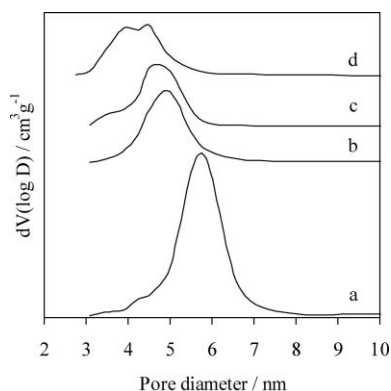


Fig. 5 BJH pore size distributions of a) SBA-15; b) MM-SBA15-1; c) MM-SBA15-2 and d) MM-SBA15-4 hierarchical macroporous-mesoporous silicas.

These textural properties are summarized in Table 1. Conventional mesoporous SBA-15 has a high specific surface area of 974 m²g⁻¹ and pore volume of 1 cm³g⁻¹, in good agreement with the literature.^{9,39,40} Comparable high surface areas are achieved for all the bi-modal MM-SBA15 materials, although the relative mesopore volume decreases from 92 to 73% with increasing macropore density, in line with expectations. The mesopore walls thicken slightly following co-templating with PS beads, demonstrating that the mesostructure is not degraded during removal of the macropore template, and may even possess greater mechanical stability than their pure mesoporous SBA-15 counterpart.

Sulfonic acid functionalization

Successful grafting of mercaptopropyl thiol groups on these macroporous-mesoporous SBA-15 analogues, and their subsequent oxidation to yield tethered sulfonic acid centres, was subsequently assessed *via* XRF, TGA and XPS (Table 2). Elemental analysis reveals the bulk S content ranges between 1.2 and 1.8 wt% across the series, increasing with total surface area. These values are typical for grafted sulfonic acid silicas,^{40,46} and equate to a sulfonic acid surface site density of ~0.24–0.35 nm⁻². In every case, surface sensitive S 2p XP spectra reveal the presence of a single sulfur chemical environment with a binding

Table 2 Sulfur and sulfonic acid content of functionalized materials evaluated by different techniques

Sample	S content ^a wt %	RSO ₃ H site density ^b /nm ²
RSO ₃ -SBA-15	1.8 (1.90)	0.35
RSO ₃ -MM-SBA15-1	1.2 (1.14)	0.22
RSO ₃ -MM-SBA15-2	1.0 (0.98)	0.20
RSO ₃ -MM-SBA15-4	1.2 (1.12)	0.24

^a TGA values shown in brackets. ^b Based on mean S content from TGA and XRF.

energy of 169.9 eV following peroxide treatment, indicative of complete thiol oxidation to sulfonic acid (Figure S5†).

TGA was also performed to quantify the sulfonic acid loading and thermal stability of untreated and functionalized silicas (Fig. 6). SBA-15 tethered mercaptopropyl groups are known to decompose by 350 °C,⁴⁷ whereas propylsulfonic acid moieties are stable until 450 °C,⁴³ at which point they decompose evolving C₃H₆, SO₂ and H₂O.⁴⁸ No major weight loss occurred below 450 °C for any of the functionalized materials, confirming complete conversion of grafted thiols into the desired sulfonic acid groups. The loss between 400 and 500 °C, and corresponding calculated total S content shown in Table 2, is in good agreement with the degree of sulfonation predicted by XRF. Although the absolute S content is expected to reflect changes in the total surface area across these different porous solids, if the inherent properties of the exposed silica surface remain identical then one would anticipate a constant surface density of grafted groups. The fall in sulfonic acid group surface density on transition from mesoporous to dual-templated SBA-15 silicas is therefore likely associated with the longer

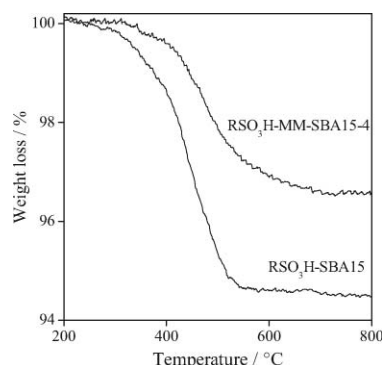


Fig. 6 TGA profiles of sulfonic acid functionalized SBA-15 and MM-SBA15-4 hierarchical macroporous-mesoporous silicas.

calcination protocol required to synthesise the MM-SBA-15 family, and concomitant lower surface hydroxyl density for subsequent thiol grafting.

It is important to note that the SBA-15 and MM-SBA15 materials retained their structural integrity post-functionalization. Porosimetry and XRD (Figures S6 and S7†) demonstrate the mesopore network is essentially unchanged by sulfonic acid grafting, while SEM confirms no impact on the longer range macroporosity (Fig. 7).

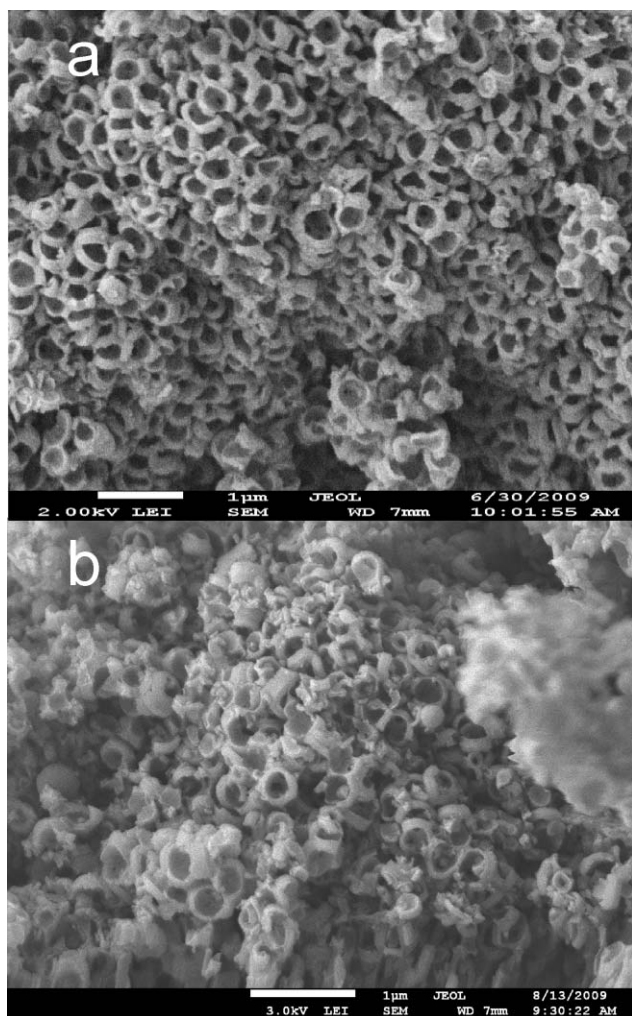
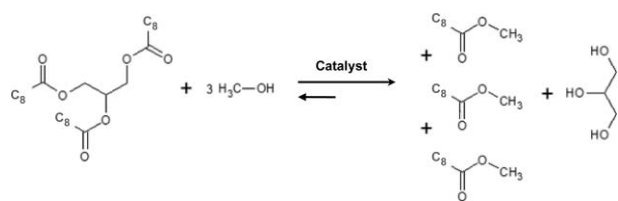


Fig. 7 SEM images of (a) as-prepared and (b) sulfonic acid functionalized MM-SBA15-4 hierarchical macroporous-mesoporous silicas.

Catalytic reactivity

The efficacy of SBA-15 and MM-SBA15 sulfonic acid silicas was subsequently evaluated towards the transesterification of tricaprylin, a bulky C_8 TAG, and separate esterification of palmitic acid (a C_{16} saturated FFA), with methanol (Scheme 1). These chemistries represent the two key steps necessary for the development of a heterogeneous biodiesel manufacturing process, namely the removal of FFA impurities and subsequent transformation of remaining TAGs through to fatty acid methyl esters.



Scheme 1 Transesterification of tricaprylin to fatty acid methyl esters and glycerol using methanol.

Steric factors render tricaprylin difficult to transesterify using conventional solid acid catalysts,^{10,49} wherein diffusion-limited kinetics are observed, making it an ideal model TAG with which to assess potential benefits of the hierarchical solid acids designed in this work. All samples proved active for tricaprylin transesterification, albeit at a low level under these mild conditions with only ~0.2 mmol converted after 6 h. Similar low conversions are common in solid acid catalysed transesterification at low temperature.^{50,51} Higher conversions were attained at elevated temperature (which necessitated autoclave operation under autogeneous conditions to prevent solvent loss), however the primary goal of this work was not to optimise FAME yields, hence of greater interest is the impact of macropores upon the initial reaction rate and concomitant turnover frequency (TOF, calculated on a per SO_3H site basis). Fig. 8 reveals a striking enhancement in the rate of transesterification as a function of increasing macropore density. The sulfonated MM-SBA15-4 material is more than twice as active as the corresponding sulfonated mesoporous SBA-15, despite its lower total surface area and pore volume. We attribute this enhanced reactivity to the greater accessibility of sulfonic acid sites within the mesopores of MM-SBA15-X materials. This improved mass-transport throughout the pore network could arise in two different ways. First, the interpenetrating macropores could simply act as large conduits to boost tricaprylin bulk diffusion throughout catalyst particles. Alternatively, by breaking up the mesopore domain size, macropore incorporation may increase the density of *accessible* sulfonic acid active sites which are likely located at the entrances to these mesopores. Smaller mesopore domains arising in the latter scenario would result in a higher *local density* of such accessible active sites per mesopore volume. In light of the strong interdependence between macropore content and mesopore domain size (the latter accounting for the majority of active surface acid sites) we cannot easily discriminate these two possible mechanisms and are therefore

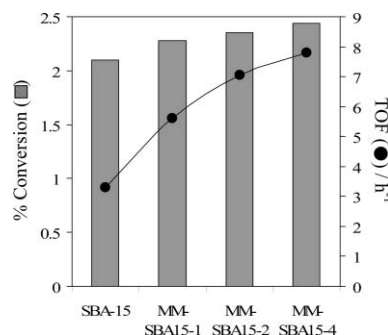


Fig. 8 Tricaprylin transesterification with MeOH over hierarchical macro-mesoporous SBA-15 sulfonic acid silicas. Conversions after 6 h at 60 °C.

currently undertaking molecular dynamics simulations to better understand and optimise TAG diffusion *via* tuning the relative macropore *versus* mesopore diameters.

Similar benefits were conferred by macropores in the esterification of palmitic acid over these hierarchical sulfonic acid silicas (Fig. 9). For all materials, conversions were far superior to those observed during the transesterification, as is well-established in the literature, reaching 55% after 6 h using the sulfonated MM-SBA15-4 catalyst. The associated TOFs reveal a similar progressive increase with rising macroporosity, with esterification proceeding 50% faster over the acid modified MM-SBA15-4 than its SBA-15 counterpart.

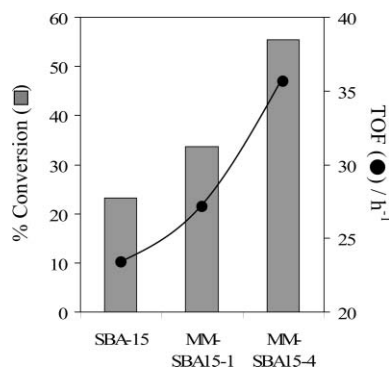


Fig. 9 Palmitic acid esterification with MeOH over hierarchical macroporous SBA-15 sulfonic acid silicas. Conversions shown after 6 h at 60 °C.

We are also investigating functionalization of this macroporous–mesoporous SBA-15 family with more active surface acid and base species to further promote plant oil transesterification and esterification.

Conclusions

Macroporous SBA-15 were synthesized *via* a simple protocol, using polystyrene bead templates, in order to improve diffusion of bulk molecules such as long-chain triglycerides and free fatty acids. PS/TEOS ratios of 2/1 and 4/1 lead to a meso-macroporous interconnected network of high specific surface area. TOFs evaluated from tricaprylin methanolysis catalysed by these sulfonic-acid functionalized silicas show that macropores enhance reactivity. These materials could provide a solution to mass-transport limitations encountered in industry when producing biodiesel from bulky plant oils *via* heterogeneous catalysis. Our preliminary study provides a new illustration of how tailoring the physical properties of solids can improve their catalytic application.

Acknowledgements

We thank the Engineering and Physical Sciences Research Council for financial support (EP/F063423/1; EP/G007594/1) and the award of a Leadership Fellowship (A.F.L.).

Notes and references

1 International Energy Agency, *World Energy Outlook 2007 - Executive Summary*, IEA publications, 2007.

- S. Pinzi, I. L. Garcia, F. J. Lopez-Gimenez, M. D. Luque de Castro, G. Dorado and M. P. Dorado, *Energy Fuels*, 2009, **23**, 2325.
- M. Lapuerta, O. Armas and J. Rodríguez-Fernández, *Prog. Energy Combust. Sci.*, 2008, **34**, 198.
- A. Demirbas, *Energy Convers. Manage.*, 2009, **50**, 14.
- K. Narasimharao, A. F. Lee and K. Wilson, *J. Bio. Mater. Bioenergy*, 2007, **1**, 19.
- A. Sivasamy, K. Y. Cheah, P. Fornasiero, F. Kemausuor, S. Zinoviev and S. Miertus, *ChemSusChem*, 2009, **2**, 278.
- Z. X. Wang, J. Zhuge, H. Fang and B. A. Prior, *Biotechnol. Adv.*, 2001, **19**, 201.
- N. R. Soriano Jr, R. Venditti and D. S. Argyropoulos, *Fuel*, 2009, **88**, 560.
- S. Miao and B. H. Shanks, *Appl. Catal., A*, 2009, **359**, 113.
- E. Lotero, Y. Liu, D. E. López, K. Suwannakarn, D. A. Bruce and J. G. Jr Goodwin, *Ind. Eng. Chem. Res.*, 2005, **44**, 5353.
- M. Di Serio, R. Tesser, L. Pengmei and E. Santacesaria, *Energy Fuels*, 2008, **22**, 207.
- M. Zabeti, W. M. A. W. Daud and M. K. Aroua, *Fuel Process. Technol.*, 2009, **90**, 770.
- E. Leclercq, A. Finiels and C. Moreau, *J. Am. Oil Chem. Soc.*, 2001, **78**, 1161.
- Y. Liu, E. Lotero, J. G. Jr Goodwin and C. Lu, *J. Catal.*, 2007, **246**, 428.
- M. Kouzu, T. Kasuno, M. Tajika, S. Yamanaka and J. Hidaka, *Appl. Catal., A*, 2008, **334**, 357; M. Verziu, B. Cojocaru, J. Hu, R. Richards, C. Ciuculescu, P. Filip and V. I. Parvulescu, *Green Chem.*, 2008, **10**, 373.
- R. S. Watkins, A. F. Lee and K. Wilson, *Green Chem.*, 2004, **6**, 335.
- J. M. Montero, P. L. Gai, K. Wilson and A. F. Lee, *Green Chem.*, 2009, **11**, 265.
- Y. Liu, E. Lotero, J. G. Jr Goodwin and X. Mo, *Appl. Catal., A*, 2007, **331**, 138; D. G. Cantrell, L. J. Gillie, A. F. Lee and K. Wilson, *Appl. Catal., A*, 2005, **287**, 183.
- K. Wilson, C. Hardacre, A. F. Lee, J. M. Montero and L. Shellard, *Green Chem.*, 2008, **10**, 654.
- D. E. De Vos and P. A. Jacobs, *Microporous Mesoporous Mater.*, 2005, **82**, 293.
- D. Zhao, Q. Huo, J. Feng, B. F. Chmelka and G. D. Stucky, *J. Am. Chem. Soc.*, 1998, **120**, 6024.
- Y. Chen, J. Han and H. Zhang, *Appl. Surf. Sci.*, 2007, **253**, 9400.
- S. Garg, K. Soni, G. M. Kumaran, R. Bal, K. Gora-Marek, J. K. Gupta, L. D. Sharma and G. M. Dhar, *Catal. Today*, 2009, **141**, 125.
- I. K. Mbaraka, D. R. Radu, V. S. Y. Lin and B. H. Shanks, *J. Catal.*, 2003, **219**, 329.
- E. Li and V. Rudolph, *Energy Fuels*, 2008, **22**, 145.
- S. Gheorghiu and M. O. Coppens, *AIChE J.*, 2004, **50**, 812.
- A. Imhof and D. J. Pine, *Nature*, 1997, **389**, 948; W. Deng, M. W. Toepke and B. H. Shanks, *Adv. Funct. Mater.*, 2003, **13**, 61; Z. Y. Yuan and B. L. Su, *J. Mater. Chem.*, 2006, **16**, 663.
- X. Zhang, F. Zhang and K. Y. Chan, *Mater. Lett.*, 2004, **58**, 2872.
- O. Sel, D. Kuang, M. Thommes and B. Smarsly, *Langmuir*, 2006, **22**, 2311.
- J. H. Sun, Z. Shan, T. Maschmeyer and M. O. Coppens, *Langmuir*, 2003, **19**, 8395.
- J. S. Yun and S. K. Ihm, *J. Phys. Chem. Sol.*, 2008, **69**, 1133.
- C. G. Oh, Y. Baek and S. K. Ihm, *Adv. Mater.*, 2005, **17**, 270.
- T. Sen, G. J. T. Tiddy, J. L. Casci and M. W. Anderson, *Chem. Mater.*, 2004, **16**, 2044.
- J. P. Blitz, and C. P. Little, *Fundamentals and Applied Aspects of Chemically Modified Surfaces*, Royal Society of Chemistry, 1999, 235.
- W. M. Van Rhijn, D. E. De Vos, B. F. Sels, W. D. Bossaert and P. A. Jacobs, *Chem. Comm.*, 1998, 317.
- W. D. Bossaert, D. E. De Vos, W. M. Van Rhijn, J. Bullen, P. J. Grobet and P. A. Jacobs, *J. Catal.*, 1999, **182**, 156.
- I. Diaz, C. Marquez-Alvarez, F. Mohino, K. Prez-Pariente and E. Sastre, *J. Catal.*, 2000, **193**, 283.
- S. Vaudreuil, M. Bousmina, S. Kaliaguine and L. Bonnevot, *Adv. Mater.*, 2001, **13**, 1311.
- D. Zhao, J. Feng, Q. Huo, N. Melosh, G. H. Fredrickson, B. F. Chmelka and G. D. Stucky, *Science*, 1998, **279**, 548.
- P. F. Siril, N. R. Shiju, D. R. Brown and K. Wilson, *Appl. Catal. A*, 2009, **364**, 95.

- 41 R. I. Kureshy, I. Ahmad, K. Pathak, N. H. Khan, S. H. R. Abdi and R. V. Jasra, *Catal. Commun.*, 2009, **10**, 572.
- 42 P. Lanzafame, S. Perathoner and G. Centi, *J. Porous Mater.*, 2007, **14**, 305.
- 43 D. Margolese, J. A. Melero, S. C. Christiansen, B. F. Chmelka and G. D. Stucky, *Chem. Mater.*, 2000, **12**, 2448.
- 44 J. J. Chiu, D. J. Pine, S. T. Bishop and B. F. Chmelka, *J. Catal.*, 2004, **221**, 400.
- 45 I. Nowak, *Col. Surfa. A*, 2004, **241**, 103.
- 46 A. F. Lee, and K. Wilson, 'Chapter 2: Sol-gel sulfonic acid silicas as catalysts' in *Handbook of Green Chemistry - Green Catalysis*, Edited by P. T. Anastas & R. H. Crabtree, Wiley-VCH, 2009, **2**.
- 47 D. Das, J. F. Lee and S. Cheng, *J. Catal.*, 2004, **223**, 152.
- 48 K. Wilson, A. F. Lee, D. J. Macquarrie and J. H. Clark, *Appl. Catal. A*, 2001, **5913**, 1.
- 49 X. Mo, D. E. López, K. Suwannakarn, Y. Liu, E. Lotero, J. G. Jr Goodwin and C. Lu, *J. Catal.*, 2008, **254**, 332.
- 50 L. Guerreiro, J. E. Castanheiro, I. M. Fonseca, R. M. Martin-Aranda, A. M. Ramos and J. Vital, *Catal. Today*, 2006, **118**, 166.
- 51 D. E. López, J. G. Jr Goodwin, D. A. Bruce and E. Lotero, *Appl. Catal. A*, 2005, **295**, 97.